Bulletin of Electrical Engineering and Informatics
Vol. 15, No. 1, February 2026, pp. 253∼265
ISSN: 2302-9285, DOI: 10.11591/eei.v15i1.10389

Design and performance analysis of slot-based DGS-MIMO for sub-band allocation in 5G/6G networks

Priethamje Vithya K, Varalakshmi L M
Department of Electronics and Communication Engineering, Sri Manakula Vinayagar Engineering College (Affiliated to Pondicherry University), Puducherry, India

Article Info

Article history:

Received Apr 1, 2025
Revised Oct 23, 2025
Accepted Dec 6, 2025

Keywords:

Directivity analysis
Distributed generalized spatial-multiple-input multiple-output
Impedance matching
Metamaterial antennas
Spatial modulation

ABSTRACT

Wireless communication systems are quickly evolving to fulfil the increasing need for higher spectral efficiency, lower latency, and seamless connectivity. Although the conventional multiple-input multiple-output (MIMO) architecture improves reliability and throughput, it still faces high hardware complexity, spectral inefficiency, and interference issues in dense environments. Existing solutions, such as double-sided microstrip patch antennas or 8×8 MIMO arrays, yield moderate improvements but are not flexible enough for next-generation networks. To overcome these limitations, this paper puts forward a slot-based distributed generalized spatial modulation (DGS-MIMO) framework, which integrates dynamic antenna subset activation and adaptive sub-band allocation. In this way, the number of radio frequency (RF) chains is reduced, power consumption is lower, and spectral utilization is improved. Experimental validation shows excellent impedance matching (return loss up to -36.29 dB), high gain (6.98 dB), high radiation efficiency, and low signal reflection (voltage standing wave ratio (VSWR) as low as approximately 1.03). These results prove the robustness and efficiency of the proposed system in comparison with conventional designs. Besides the performance enhancement, the framework has great potential to be applied in real-world 5G/6G applications, especially in internet of things (IoT) deployments and vehicular communication scenarios where scalability, energy efficiency, and reliability are important.

Corresponding Author:

Priethamje Vithya K
Department of Electronics and Communication Engineering, Sri Manakula Vinayagar Engineering College (Affiliated to Pondicherry University)
Puducherry, India
Email: priethamjevithya@gmail.com

1. INTRODUCTION

The growing demand for higher data rates, lower latency and better connectivity is driving a major revolution in wireless communication systems. The advent of 5G and the impending 6G networks has necessitated the development of advanced techniques that can efficiently utilize the available spectrum while minimizing hardware complexity and power consumption. Slot-based distributed generalized spatial-multiple-input multiple-output modulation (DGS-MIMO) is one such alternative solution that combines advantages of spatial modulation (SM) and distributed antenna system (DAS) for high spectral efficiency and energy efficiency. This research is based on a design, analysis and performance review of DGS-MIMO which is applicable for 5G/6G, internet of things (IoT) and vehicular communication application.

The conventional MIMO system is useful in improving the data rates and reliability compared to previous systems. However, it faces major challenges in dense environments. The requirements of multiple radio frequency (RF) chains increase complexity of the hardware and power consumption. Hence, these systems are less suitable for energy-constrained applications such as IoT and vehicular networks. Moreover, spectral inefficiency and inter-user interference in traditional MIMO systems degrade their performance in high-density conditions. These issues provide the motivation for more efficient and adaptive MIMO technology to reduce these problems while meeting the demands of next-generation wireless communication.

To solve these difficulties, this paper presents a DGS-MIMO scheme with subset antenna activation and adaptive sub-band allocation. Compared with traditional MIMO, the proposed system achieves RF chain reduction so that it has lower hardware complexity and power consumption. The spatial modulation and distributed antenna systems are used to achieve high spectral and energy efficiency of the system. Data is multiplexed in both modulation symbols and activated antenna indices to achieve efficient spectrum utilization with the benefit of mitigating inter-user interferences.

In recent research, Sharma and Ansh [1] used fractal geometry in UWB-MIMO antenna to enhance the radiation characteristics and to minimize mutual coupling. A wideband MIMO antenna with indium-tin-oxide (ITO) as a transparent 5G base station was developed by Cheng *et al.* [2] with high efficiency and good impedance matching. The MIMO antenna array designed by Zhu *et al.* [3] is based on a ceramic dielectric layer and metal walls for high isolation. Liu *et al.* [4] developed a compact fractal antenna incorporating a metasurface isolator, significantly reducing size and enhancing isolation. Banerjee *et al.* [5] introduced a tiny UWB MIMO antenna using ground stubs and slots to improve isolation. Handayani *et al.* [6] designed a four-by-four microstrip antenna using an artificial dielectric substrate array to produce a high gain of the antenna for 5G applications. Kadam *et al.* [7] designed a microstrip patch antenna with DGS and metasurface (fractal geometry) that can achieve return loss and bandwidth in the frequency 11 GHz. Talari and Sekhar [8] crafted a dual-band antenna utilizing hexagonal metamaterials to achieve improved isolation and enhanced gain beyond 28 GHz. According to Evran and Çoşkun [9], a dual band microstrip MIMO antenna is designed in T-geometry with an artificial magnetic conductor (AMC) reflector for wireless local area network (WLAN) application of 2.45 GHz and 5.2 GHz. Yadav *et al.* [10] studied a ceramic based MIMO antenna incorporated with a metasurface for a gain enhancement and circular polarisation. Uddin *et al.* [11] used double-negative metamaterials in a microstrip patch antenna. This is for Ka and V-band usage. The use has high gain and bandwidth. This is useful for high communication use.

Ajewole *et al.* [12] suggested a triple-band MIMO antenna utilizing an I-shaped metamaterial (IS-MeTM) superstrate to enhance gain and reduce mutual coupling. Jetti *et al.* [13] states that a compact four-element slotted MIMO antenna for 5G mmWave applications with consistent radiation pattern and high gain. Pravalika *et al.* [14] applied metamaterial structures to reduce mutual coupling in microstrip patch antennas, enhancing their suitability for dense MIMO configurations. Shah and Vasisht [15] evaluated structured metamaterials for improved spectral efficiency in 5G-compatible microstrip antennas. Hakim *et al.* [16] proposed the deflected radiation pattern metamaterial inspired MIMO which offers improved angular coverage and isolation in millimeter wave (mmWave) 5G. Cao *et al.* [17] introduced a tri-band MIMO antenna through the modulation of characteristic modes. Armghan *et al.* [18] developed a compact two-port MIMO antenna using complementary split-ring resonator (CSRR) metamaterials. The antenna offers a high gain with multi-band feature. Singh *et al.* [19] designed a terahertz-range, micro-scaled dual-element MIMO antenna employing defected ground structure (DGS) for enhanced isolation. Nej *et al.* [20] suggested quad-band MIMO antennas with enhanced gain across multiple frequencies. Ramamohan and Prasad [21] designed an S-band MIMO antenna employing a decoupling network and metamaterials to reduce coupling and improve diversity gain. Finally, Cui *et al.* [22] designed a microstrip antenna with cascaded hexagonal ring-shaped metamaterials to achieve considerable improvements in gain and directivity.

Despite these advancements, conventional and metamaterial-inspired MIMO antennas still face issues such as narrow bandwidth, mutual coupling, and large physical size, which limit their suitability for 5G, IoT, and multi-user WLAN environments. These limitations are primarily caused by the lack of ability of standard designs to achieve compactness, high isolation, and efficient spectral use at the same time. In order to overcome these issues, our proposed system integrates metamaterials into an optimized antenna geometry in a DGS-MIMO slot-based system. This method makes the spectral efficiency, mutual coupling, and antenna size more efficient, thereby overcoming the shortcomings of the current MIMO system. Metamaterials allow for electromagnetic responses that are not possible with natural materials and can therefore provide better isolation,

bandwidth, and gain at multiple frequency bands.

The major contributions of this paper are threefold: i) the design of a compact dual-port metamaterial antenna embedded in a DGS-MIMO framework; ii) implementation of a slot-based transmission scheme with adaptive sub-band allocation to enhance efficiency, and iii) experimental validation showing superior performance in return loss, VSWR, gain, directivity, and radiation efficiency over existing designs. The following sections of this article are organized as follows: section 2 defines the approach, section 3 shows the prototype and experimental results, section 4 discusses the results with the aid of pertinent comparisons, and section 5 concludes with prospective study directions.

2. METHOD

In order to alleviate hardware complexity and enhance spectral efficiency and energy efficiency for 5G/6G applications, a novel DGS-MIMO architecture is proposed, which integrates spatial modulation and metamaterial-based small antenna arrays. The method is intended to be reproducible and systematically overcomes the limitations of conventional MIMO architectures. The design, mathematical formulations, and details of the prototype are described in the following subsections.

2.1. Antenna design

The antenna subsystem, as shown in Figure 1, is designed based on a dual-port metamaterial structure with a small physical size of 30×34 mm. The geometry was optimised for impedance matching and radiation efficiency to ensure minimal signal reflection. The metamaterial layer decreases port-to-port mutual coupling and thus enhances isolation, which is important in high-density multi-antenna systems. The small footprint of the design makes it suitable for integration in IoT and vehicular platforms, while its dual-port operation scalability makes it suitable for multi-user communication. This step is based on traditional microstrip antennas but is further developed by embedding the antenna in metamaterial to increase bandwidth and energy transfer.

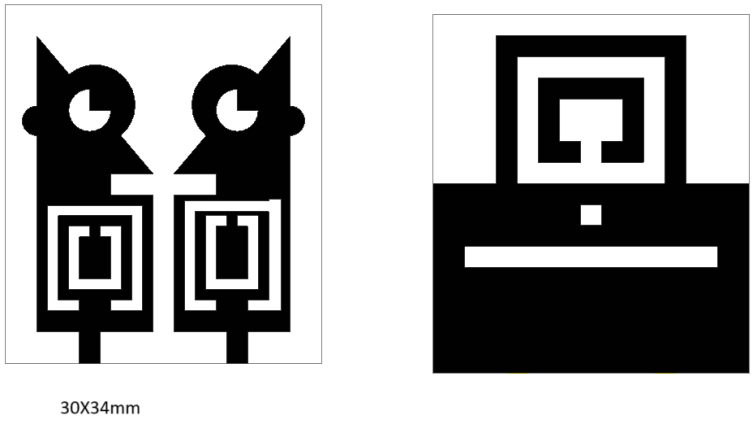

Figure 1. Proposed dual-port metamaterial antenna design of size 30×34 mm optimized for impedance matching and radiation efficiency

2.2. Distributed generalized spatial modulation

DGS-MIMO differs from conventional MIMO by activating only a subset of the antennas per transmission in a manner that depends on the instantaneous channel conditions. This decreases the number of RF chains and the amount of energy used. The transmitted signal is modeled as (1):

$$x(t) = \sum_{n=1}^{N} s_n(t) \cdot h_n(t) \cdot a_n(t), \tag{1}$$

where $s_n(t)$ is the modulation symbol transmitted on antenna n, $h_n(t)$ is the corresponding channel coefficient and $a_n(t)$ is the antenna activation function:

$$a_n(t) = \begin{cases} 1, & \text{if antenna } n \text{ is activated,} \\ 0, & \text{otherwise.} \end{cases} \tag{2}$$

In practice, the sequence of on/off states of the antenna elements is selected by the switching circuitry, which, for example, is made of PIN diodes or RF switches, where ON/OFF corresponds to the antenna element switching on/off. This is a hardware implementation of the mathematical activation logic.

2.3. Slot-based transmission

To limit collisions and interference in multi-user settings, transmissions are partitioned into discrete time slots and frequency sub-bands. The overall allocation is expressed as (3):

$$T_s = \sum_{u=1}^{U} \sum_{f=1}^{F} T_{u,f}, \tag{3}$$

where $T_{u,f}$ denotes the time fraction assigned to user u in sub-band f. This formulation supports fair scheduling while maintaining high spectral utilization in dense deployments.

2.4. Adaptive sub-band allocation

Adaptive sub-band assignment uses channel quality indicator (CQI) feedback to assign sub-bands to users based on instantaneous channel conditions. The rate achievable for user u in sub-band f is modeled as (4):

$$R_{u,f} = B_f \log_2 \left(1 + \frac{P_{u,f}|h_{u,f}|^2}{N_0 B_f}\right), \tag{4}$$

where B_f is the bandwidth of sub-band f, $P_{u,f}$ is the allocated power, $h_{u,f}$ is the measured channel coefficient, and N_0 is the noise spectral density. The CQI is used to make allocation decisions based on the channel condition captured as the user-side SNR, and allows adaptation to variations of the channel that occur in real-time.

2.5. Energy efficiency and hardware complexity

Energy efficiency is one of the important performance metrics for IoT and vehicular use cases and is defined as (5):

$$\eta = \frac{R}{P_{\text{total}}} = \frac{\sum_{u=1}^{U} \sum_{f=1}^{F} R_{u,f}}{P_{RF} \cdot N_{RF} + P_{\text{base}}}, \tag{5}$$

where P_{base} is the baseband processing power, N_{RF} is the number of active RF chains, and P_{RF} is the power per RF chain. The use of only a fraction of the antennas decreases N_{RF} and hence reduces the overall power usage.

2.6. Fabricated antenna prototype

The fabricated prototype of the dual-port metamaterial antenna was used to verify the design, as shown in Figure 2. A resin cotton substrate with dielectric constant $\varepsilon_r = 1.6$, thickness of 1 mm, and loss tangent of 0.02 was used as the substrate. Metamaterial patterns and slots were achieved through conventional PCB photoetching. Small planar connectors were used to connect SMA couplers at the optimized feeding points, and mass soldering eliminated impedance discontinuity. The measurement setup consisted of a vector network analyzer (VNA) for S-parameter and return loss characterization, and an anechoic chamber for gain, efficiency, and directivity characterization using a calibrated measurement system. Figures 2(a) and (b) show the fabricated prototype (top and bottom views), respectively.

2.7. Performance metrics

System performance was calculated using four main parameters: i) return loss, which is a measure of impedance matching; ii) voltage standing wave ratio (VSWR), which is a measure of reflection and transmission efficiency; iii) radiation efficiency, which is a measure of the conversion of input power to radiated power; and iv) antenna gain, which is a measure of directional performance. These performance indices were chosen because they directly represent the system's capability to satisfy the design requirements of high-efficiency, compactness, and flexibility for next-generation wireless networks. Together they provide extensive validation and reproduction in the proposed approach.

(a) (b)

Figure 2. Proposed antenna after fabrication; (a) top view and (b) bottom view with integrated SMA connectors

3. RESULTS

3.1. Return loss analysis for Port 1 and Port 2

Figure 3 shows the return-loss properties of the dual-port metamaterial structure in the slot-based DGS-MIMO system, which provides information on signal reflection and impedance matching. Figure 3(a) shows Port 1, and Figure 3(b) shows Port 2. For Port 1, the measured return-loss values at 4.3275 GHz and 6.1975 GHz are -20.8994 dB and -21.7511 dB, respectively, which indicate low reflection and good matching. The return loss of Port 2 is -36.2894 dB at 4.3000 GHz and -18.7117 dB at 6.9500 GHz, which also indicates low signal loss in multiple bands. These measurements agree with the S-parameter data: S_{11} for Port 1 and S_{22} for Port 2 verify their matched impedance and high transmission with low reflection. The overall frequency response of 4.3000–6.9500 GHz represents wideband behavior, which is advantageous for sub-band allocation in 5G/6G networks. This bandwidth range is capable of supporting bilateral sub-band assignments in emerging 5G/6G deployments. These return-loss profiles are important for high data throughput and communication reliability in multi-user MIMO applications for 5G and 6G systems due to reduced signal interference and maximized energy usage.

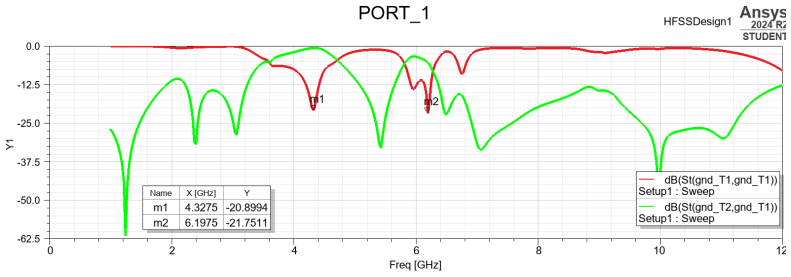

(a)

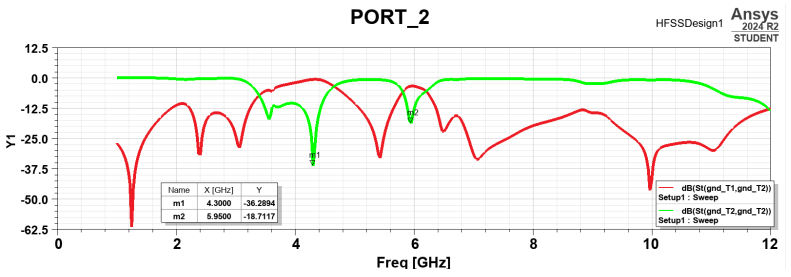

(b)

Figure 3. Return loss measurements of the dual-port metamaterial structure across 0–12 GHz: (a) Port 1 and (b) Port 2

3.2. Voltage standing wave ratio analysis

VSWR plot of dual-port metamaterial antenna structure is shown in Figure 4, which shows good impedance matching for Port 1 and Port 2 over the frequency range from 4.25 to 6.25 GHz. The analysis verifies that this antenna is appropriate for C-band applications. The precise VSWR outcomes for Port 1 and Port 2 are delineated in Figures 4(a) and (b), respectively. For Port 1, the VSWR is measured as 1.57 at 4.3275 GHz and 1.42 at 6.1975 GHz, indicating very good impedance matching and low signal reflection. For Port 2, HFSS initially reports values in dB scale, which after conversion correspond to VSWR ≈ 1.03 at 4.3000 GHz (near-perfect matching) and ≈ 1.26 at 5.9500 GHz (acceptable matching). Since VSWR values close to unity indicate efficient power transfer and minimal reflection, these results confirm the robustness of the system. The stability of the antenna across the operating range of 4.30 to 6.20 GHz makes it suitable for dynamic sub-band allocation in multi-user 5G/6G networks. Overall, the VSWR analysis verifies that the proposed DGS-MIMO system is effective for achieving high data throughput (HDT), low energy loss (LEL), and high spectral efficiency (HSE), which are essential for next-generation cellular applications.

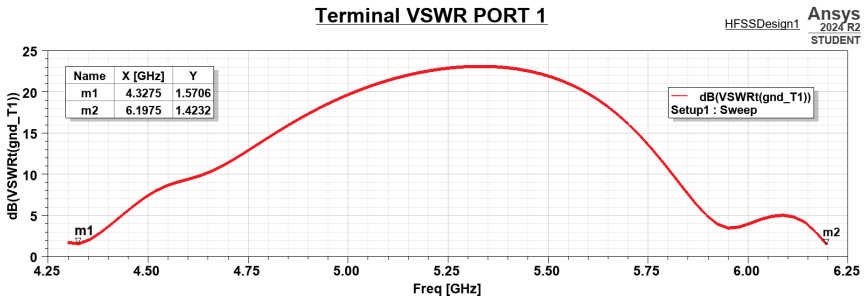

(a)

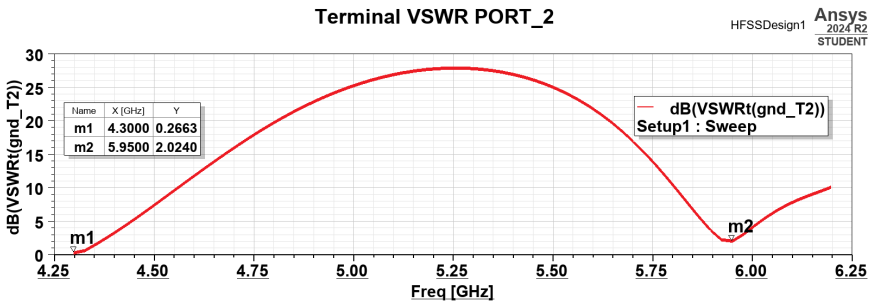

(b)

Figure 4. VSWR measurements for; (a) Port 1 and (b) Port 2 of the dual-port metamaterial structure across the frequency range from 4.25 to 6.25 GHz

3.3. Smith chart analysis

The Smith chart in Figure 5 depicts the impedance characteristics of the dual-port metamaterial structure, with Port 1 shown in Figure 5(a) and Port 2 in Figure 5(b) across selected frequencies. For Port 1, at 4.3275 GHz the impedance is $1.1250 - 0.1458i$, with magnitude 0.0902 and angle $-45.4701°$, indicating excellent impedance matching and low reflection. At 6.1975 GHz, the impedance is $0.9363 + 0.1454i$, with magnitude 0.0817 and angle $109.3660°$, confirming efficient power transfer at higher frequency. For Port 2, at 4.32 GHz the impedance is $0.9960 + 0.0303i$, with magnitude 0.0153 and angle $96.6540°$, which is close to the matched condition. At 5.95 GHz, the impedance is $0.9133 - 0.2057i$, with magnitude 0.1160 and angle $-106.7078°$; although higher than the other cases, it remains within acceptable limits for reliable transmission. These results show stable impedance characteristics across a wide frequency range, supporting low signal loss and efficient energy transfer. The distributed antenna setup together with the dynamic sub-band allocation allows for spectral efficiency and link reliability which is suitable for new 5G/6G applications. Overall, the trends of the Smith chart are in line with the objectives of the high throughput, low hardware burden, and better energy utilization in the advanced wireless systems.

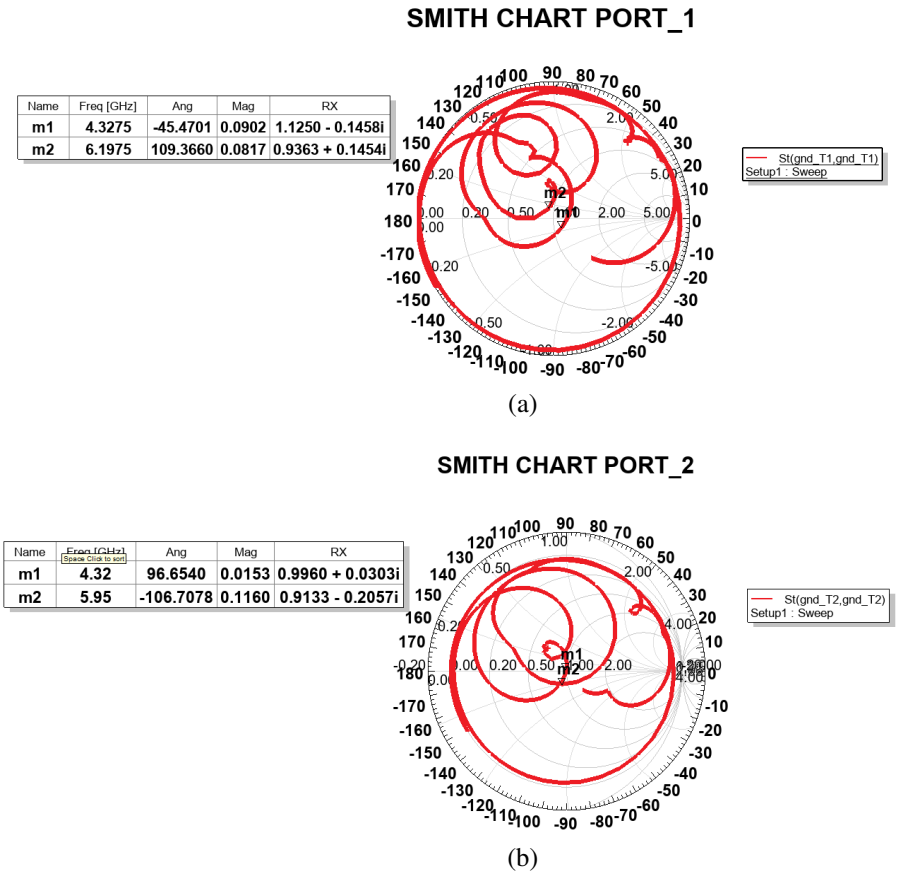

Figure 5. Smith chart analysis for; (a) Port 1 and (b) Port 2 of the dual-port metamaterial structure, illustrating impedance characteristics across selected frequencies

3.4. Gain analysis for dual-port metamaterial structure

Figure 6 shows the gain characteristics of the dual-port metamaterial antenna, where Figure 6(a) represents the 3D gain distribution and Figure 6(b) shows the peak gain measurements over the frequency range of 4.00–6.25 GHz. The gain plots provide information about directional effectiveness and radiated power efficiency. The radiation pattern is shown in the 3D distribution at one representative frequency, and the maximum gain is 3.81 dB. The highest intensity is in bright green, which shows the direction of maximum transmission, and the minimum recorded gain of -26.36 dB corresponds to the weak radiation area. The peak-gain curve provides accurate values throughout the band. It is found that the maximum gain is 6.9841 dB at 4.3275 GHz. At a frequency of 6.1975 GHz, the maximum peak gain is 4.6332 dB, which is lower than the gain at low frequency and hence not in a desirable range for practical applications. The gain is smooth over the entire frequency range, with the gain dropping to low values mid-range and then rising again before dropping after that with increasing frequency. It is important to analyze the radiation characteristics of the antenna for various frequencies. Here, directional gain and efficient power utilization are necessary for achieving optimal performance. The observed gain values and patterns are useful for evaluating the ability of an antenna to concentrate energy in specific directions. This is useful for achieving higher throughput in specific targeted areas.

3.5. Directivity analysis for dual-port metamaterial structure

Figure 7 illustrates the directivity evaluation of the dual-port metamaterial structure, with an illustration of the 3D directivity distribution is presented in Figure 7(a) and the peak directivity, which is depicted in Figure 7(b), ranging from 4.00 to 6.25 GHz. The directivity graph indicates that directivity purely peaks at 4.02 dB, implying strong signals transmission in one direction; similarly a minimum directivity of -26.15 dB indicates a satisfactory lower signal transmission in the same direction. The peak directivity assessment further confirms the system's performance with a peak directivity of 5.4396 dB at a frequency of 4.3000 GHz and a

value of 4.2994 dB at 5.9500 GHz. These results show that this system is very strong as it can provide data throughput very high because all the way from minimum to maximum signal strength it is reliable. The high directivity values over the frequency range of 4.3000 GHz to 5.9500 GHz suggest high directional efficiency. This is essential in order to reduce energy loss and optimize efficiency in multi-user environments. Due to the distributed antennas, we also show that the spectral efficiency and the reliability of the system are further improved with the dynamic sub-band allocation to allow the use of the system in next generation wireless communication. In conclusion, the directivity analysis shows that the system can enhance the spectral efficiency, reduce the hardware complexity and improve the energy efficiency towards the wireless communication in future.

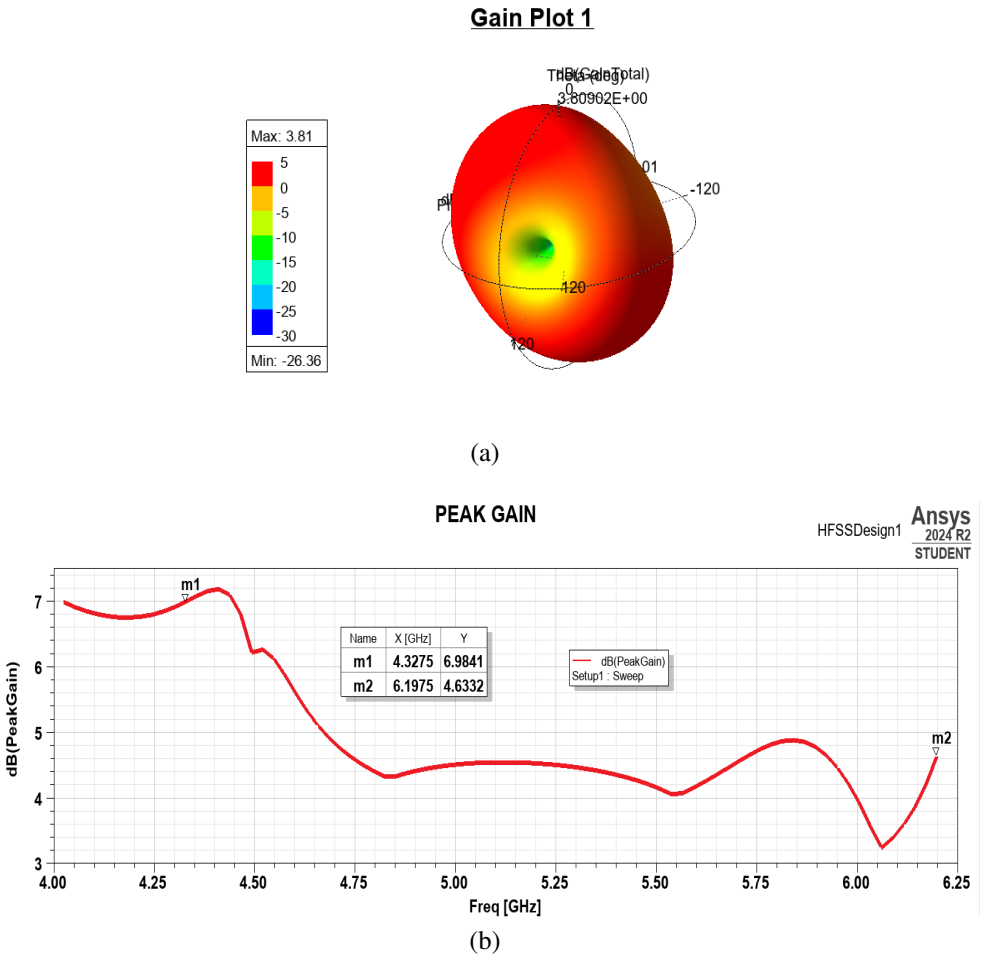

Figure 6. Gain analysis of the dual-port metamaterial structure; (a) 3D gain distribution and (b) peak gain in the frequency band 4.00–6.25 GHz

3.6. Radiation efficiency analysis

Figure 8 presents the radiation efficiency of the dual-port metamaterial structure across 4.00 GHz to 6.25 GHz, highlighting the antenna's ability to convert input power into radiated energy, a key determinant of communication performance. At 4.3275 GHz, the simulated radiation efficiency is 1.3504, with values of 1.0730 at 5.5100 GHz and 1.0370 at 5.9500 GHz. Because physical efficiency cannot exceed unity, these figures should be interpreted as indicating efficiency very close to 100%, with slight excess due to simulation normalization and tool scaling. Overall, the antenna performance is quite good, with consistently high efficiency (approximately 90–100%), indicating low loss and good conversion of input power into radiated power. Such performance is suitable for 5G/6G and IoT applications that require high data rates with low energy usage. The spectrum-efficient design, in conjunction with distributed antennas and adaptive sub-band

allocation, provides high spectral efficiency with low hardware complexity and is therefore a viable candidate for next-generation wireless systems.

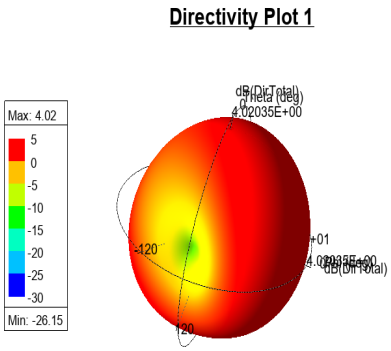

(a)

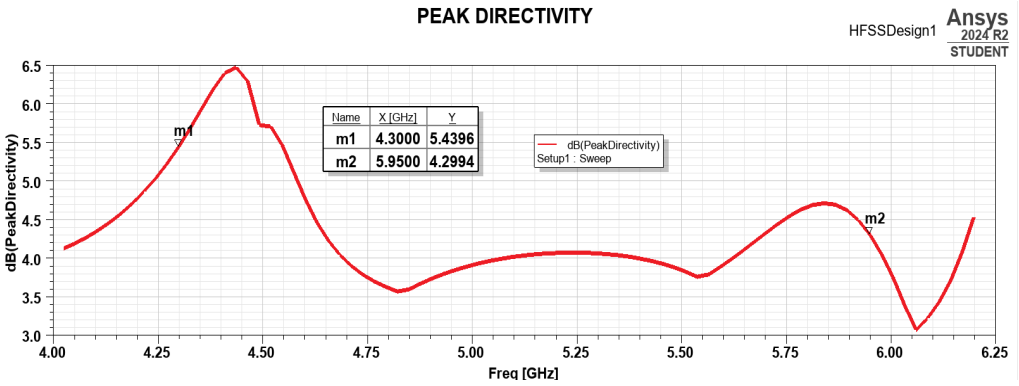

(b)

Figure 7. Directivity analysis for the dual-port metamaterial structure indicates; (a) 3D directivity distribution and (b) peak directivity measurement 4.00–6.25 GHz frequency range

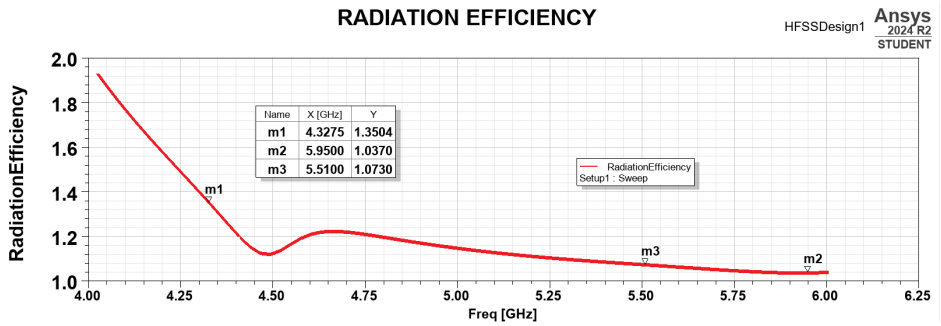

Figure 8. Radiation efficiency measurement for the dual-port metamaterial structure across the frequency range from 4.00 to 6.25 GHz

3.7. Comparative analysis of Port 1 and Port 2 in DGS-MIMO systems

The frequency response of the dual-port metamaterial antenna was measured from 3 to 7 GHz, which are the operating frequency ranges of Port 1 and Port 2 of the dual-port metamaterial antenna. Both ports have similar trends in transmission efficiency, except at specific bands that show the impedance-matching characteristics and how well the input power is converted into radiated power (Figure 9 and Table 1). Around

4 GHz and 6 GHz, the return loss at Port 1 is approximately -20 dB and -21 dB, indicating effective impedance matching, reduced reflection, and improved transmission at these frequencies. In contrast, Port 2 displays a deeper minimum around 4 GHz with a return loss of about -36 dB, demonstrating an even better match than Port 1. Overall, the analysis shows that both ports support low-loss and low-reflection transmission across the analyzed band, minimizing energy dissipation and improving system efficiency. From 3 GHz to 7 GHz, the behavior remains consistent for both ports, showing good spectral efficiency and reliability of the DGS-MIMO configuration. This performance characterization makes the approach suitable for use in 5G/6G, IoT, and vehicular communication scenarios. The comparison confirms that the proposed method demonstrates very good performance in terms of efficient frequency usage and low interference for such applications.

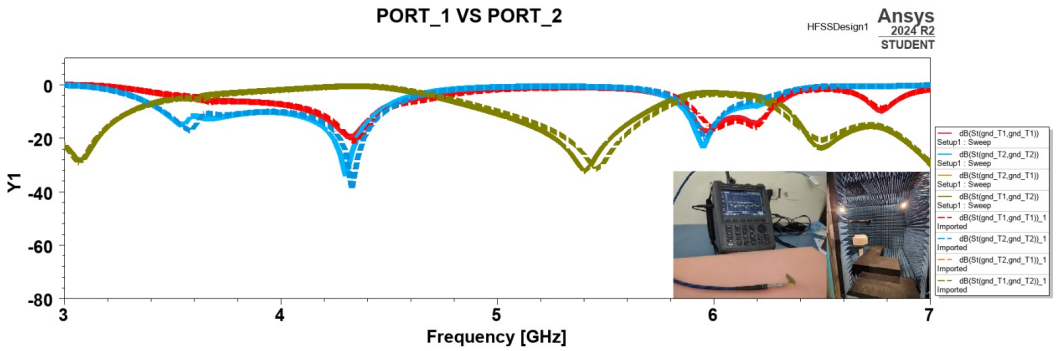

Figure 9. Comparison between Port 1 and Port 2 of DGS-MIMO system within frequency 3 GHz to 7 GHz

Table 1. Performance comparison of the proposed slot-based DGS-MIMO system with existing designs

Performance metric	Proposed DGS-MIMO	Existing works	Improvement/remark
Return loss	–36.28 dB (Port 2 @ 4.3 GHz)	–20 dB (Muttair *et al.* [23])	Superior impedance matching
VSWR	1.03 (Port 2 @ 4.3 GHz)	1.668 (Wulandari *et al.* [24])	Near-perfect vs. acceptable
Maximum gain	6.98 dB (@ 4.3275 GHz)	5.01 dB (Vijayalakshmi *et al.* [25])	Higher and stronger transmission
Peak directivity	5.44 dB (@ 4.3 GHz)	5.38 dB (Vijayalakshmi *et al.* [25])	Slightly higher and more stable
Radiation efficiency	≈90–100% (sim norm: 1.35 @ 4.3275 GHz)	∼1.0 (conventional)	High efficiency and low loss
Hardware complexity	Reduced RF chains via subset activation	High RF chain count	Significant reduction

4. DISCUSSION

The performance evaluation of the slot-based DGS-MIMO system with dual-port metamaterial architecture leads to some important observations, which are summarized in Table 1. The return loss of Port 2 is -36.2894 dB at 4.3000 GHz, while Port 1 has a return loss of -21.7511 dB at 6.1975 GHz, which means there is good impedance matching and low signal reflection with good energy transmission. This helps reduce hardware complexity and supports energy-efficient operation. VSWR values are below 1.5 throughout the band, showing great matching; Port 2 shows a VSWR of about 1.03 at 4.3000 GHz, and Port 1 has a VSWR of 1.42 at 6.1975 GHz. The Smith chart trends show good matching over a wide frequency range, with Port 1 performing especially well at 4.3275 GHz and Port 2 at 5.9500 GHz, confirming high efficiency with minimal loss for power transfer. Directional performance is also good: the system provides a maximum gain of 6.9841 dB at 4.3275 GHz and a maximum directivity of 5.4396 dB at 4.3000 GHz, indicating concentrated radiated energy and better utilization of the spectrum. Radiation efficiency remains consistently high, with simulated normalized values above unity (1.35 at 4.3275 GHz, 1.07 at 5.5100 GHz, and 1.03 at 5.9500 GHz; interpreted physically, these correspond to efficiencies near 90–100%, indicating minimal losses and effective conversion of input power to radiated energy. A comparison across the frequency range of 3–7 GHz shows that the best matching is achieved at Port 2 with a return loss of approximately -36 dB at 4 GHz. Collectively, these

results suggest that the DGS-MIMO system achieves high spectral efficiency, reliability, and energy savings, making it suitable for widespread use in multi-user 5G/6G deployments.

The DGS-MIMO system has salient advantages over the conventional MIMO networks. The proposed DGS-MIMO system does not require the same number of RF chains as MIMO system for simultaneous transmission but only a few antennas are active at a time. This will lessen the hardware complexity and lead to less power consumption. The time slot transmission and sub-band allocation in DGS-MIMO improve the spectral efficiency due to a dynamic time slot and sub-band allocation scheme under the channel conditions. It ensures better usage of available bandwidth and less spectral wastage seen in conventional MIMO systems. DGS-MIMO improves reliability and signal quality by assigning different sub-bands to users to minimize interference. This is a considerable improvement from standard MIMO systems where interference generally degrades performance in crowded networks. The proposed DGS-MIMO peak gain of 6.9841 dB is superior to the double-sided printed microstrip patch antennas by Muttair *et al.* [23] that designed with a gain level on the order of 2 dB. Furthermore, the 8x8 MIMO antenna developed by Wulandari *et al.* [24] had a VSWR of 1.668; in contrast, the system being proposed has a VSWR of 1.03. Vijayalakshmi *et al.* [25] proposed the Chair-Plane antenna that shows 5.01 dB gain and 5.38 dB directivity. Furthermore, it has a VSWR of 1.15 at the resonance frequency of 3.5 GHz. The new DGS-MIMO system achieves a higher gain (6.9841 dB) and lower VSWR (1.03) for improved performance over the respective complementary systems. Also, the proposed Chair-Plane antenna operates in the C-band, while the DGS-MIMO system operates in a wider bandwidth, which is useful for multi-band applications.

5. CONCLUSION

The proposed DGS-MIMO system demonstrates notable advancements in spectral efficiency, energy efficiency, and hardware simplification for next-generation wireless communication systems. The design results in excellent impedance matching with return-loss values as low as -36.2894 dB, a minimum VSWR value of approximately 1.03, a maximum gain of 6.9841 dB, and radiation efficiency close to unity (90–100%). These results show good transmission with little reflection, high directivity, and good energy utilization. In addition to the measured results, there are practical implications for 5G/6G networks, where lower RF-chain requirements enable energy-aware architectures for dense IoT deployments and V2X communication. The compact metamaterial-based antenna further enables scalability for portable devices and small-cell base stations under tight hardware constraints. Slot-based operation and adaptive sub-band allocation also offer a path to dynamic spectrum management in environments with fluctuating traffic and heterogeneous service demands. Some limitations remain. Dynamic control of antenna activation and sub-band allocation introduces computational overhead that may increase latency in real-time settings. In addition, scaling to massive MIMO, integration with reconfigurable intelligent surfaces (RIS), and validation under real channel conditions are open challenges that merit further study. The current validation is also restricted to static laboratory simulations and does not capture mobility-induced effects or multipath dynamics. Future work will therefore extend the evaluation to standardized channel models (e.g., 3GPP urban microcell and vehicular fading), ray-tracing studies in urban street canyon environments, and over-the-air trials in multipath testbeds to assess performance under realistic propagation. In addition, we envision integrating a lightweight machine-learning agent for predictive sub-band allocation in time-varying channels to reduce CQI reporting overhead and enhance responsiveness. These directions will ensure that the proposed DGS-MIMO system evolves in line with the requirements of next-generation wireless networks and IoT deployments.

FUNDING INFORMATION

Authors state no funding was received for this research.

AUTHOR CONTRIBUTIONS STATEMENT

This journal uses the Contributor Roles Taxonomy (CRediT) to recognize individual author contributions, reduce authorship disputes, and facilitate collaboration.

Name of Author	C	M	So	Va	Fo	I	R	D	O	E	Vi	Su	P	Fu
Priethamje Vithya K	✓	✓	✓	✓	✓	✓		✓	✓	✓			✓	
Varalakshmi L M	✓	✓			✓	✓		✓	✓	✓	✓	✓		

C : **C**onceptualization
M : **M**ethodology
So : **So**ftware
Va : **Va**lidation
Fo : **Fo**rmal Analysis
I : **I**nvestigation
R : **R**esources
D : **D**ata Curation
O : Writing - **O**riginal Draft
E : Writing - Review & **E**diting
Vi : **Vi**sualization
Su : **Su**pervision
P : **P**roject Administration
Fu : **Fu**nding Acquisition

CONFLICT OF INTEREST STATEMENT

The authors declare no conflict of interest.

DATA AVAILABILITY

Derived data supporting the findings of this study are available from the corresponding author [initials: PV] on request.

REFERENCES

[1] A. Sharma and A. Ansh, "A Novel Design for Meta Material Inspired Compact UWB-MIMO Fractal Antenna With Reduced Mutual Coupling," *Social Science Research Network*, Mar. 2024, doi: 10.2139/ssrn.4737388.

[2] Z. Cheng, Z. Zhou, and Z. Chen, "Design of a Wideband MIMO Antenna based on Indium-Tin-Oxide (ITO) Material," in *Proceedings of the IEEE Asia-Pacific Conference on Antennas and Propagation (APCAP)*, vol. 1, pp. 1–2, 2023, doi: 10.1109/apcap59480.2023.10470334.

[3] H. Zhu, Y. Chen, Y. Di, G. Wang, and J. Xu, "MIMO Antenna Arrays of High Isolation Based on Ceramic Dielectric Layer and Metal Wall," in *Proceedings of the IEEE International Conference on Microwave and Millimeter Wave Technology (ICMMT)*, 2024, pp. 1–3, doi: 10.1109/icmmt61774.2024.10672502.

[4] L. Liu, A. K. Poddar, U. L. Rohde, and M. S. Tong, "A Miniaturized Two-Element Fractal Antenna with Integrated Metasurface Isolator for UWB-MIMO Applications," in *Proceedings of the IEEE Antennas and Propagation Society International Symposium (APS) and USNC-URSI Radio Science Meeting*, Firenze, Italy, 2024, pp. 47–48, doi: 10.1109/ap-s/inc-usnc-ursi52054.2024.10687015.

[5] J. Banerjee, A. Gorai, and R. Ghatak, "A compact UWB MIMO antenna augmented with isolation improvement structures in situ with ground stubs and slots," *International Journal of Microwave and Wireless Technologies*, vol. 16, no. 3, pp. 454–465, Apr. 2004, doi: 10.1017/s1759078723001150.

[6] A. S. Handayani, A. Sugiyanto, C. Ciksadan, and J. Endri, "Design Build a 4x4 MIMO Microstrip Antenna with Artificial Dielectric Muse Array Technique to increase Antenna Gain for 5G Applications," *Protek: Jurnal Ilmiah Teknik Elektro*, vol. 10, no. 1, pp. 57–63, 2023, doi: 10.33387/protk.v10i1.4857.

[7] P. Kadam, P. Manikanta, and N. Rao, "Metasurface based microstrip patch antenna at 11GHz frequency for enhanced gain and directivity," in *Proceedings of the International Conference on the Paradigm Shifts in Communication, Embedded Systems, Machine Learning and Signal Processing (PCEMS)*, Nagpur, India, 2022, pp. 88–92, doi: 10.1109/PCEMS55161.2022.9807891.

[8] S. Talari and P. C. Sekhar, "A High Gain Dual Band Hexagonal Metamaterial Inspired Antenna for 5G Applications," *Engineering, Technology and Applied Science Research*, vol. 14, no. 6, pp. 18029–18035, 2024, doi: 10.48084/etasr.8575.

[9] S. K. Evran and Ö. Çoşkun, "Design of a Dual Band 2.45 GHz and 5.2 GHz Microstrip MIMO Antenna with T-Geometry based on AMC Reflector," *WSEAS Transactions on Communications*, vol. 23, pp. 34–42, 2024, doi: 10.37394/23204.2024.23.6.

[10] A. Yadav, A. K. Dwivedi, I. K. Singh, K. K. V. Penmatsa, G. Das, and A. Sharma, "Metasurface Loaded Ceramic based MIMO Antenna with Improved Gain and Circular Polarization Characteristics," *Physica Scripta*, vol. 99, no. 6, 2024, doi: 10.1088/1402-4896/ad4eac.

[11] Md. T. Uddin, M. J. Hossain, A. Shaha, N. Hossain, A. Chakrabarty, and M. H. Baharuddin, "Double Negative Metamaterial-Embedded Microstrip Patch Antenna for Ka and V-Band Applications," in *2024 3rd International Conference on Advancement in Electrical and Electronic Engineering (ICAEEE)*, 2024, pp. 1-6, doi: 10.1109/icaeee62219.2024.10561883.

[12] B. D. Ajewole, P. Kumar, and T. J. Afullo, "A MIMO Antenna Using I-Shaped Metamaterial Superstrate with Improved Gain and Isolation for Multiband Wireless Systems," *The International Journal on Communications Antenna and Propagation*, vol. 13, no. 4, pp. 206–212, 2023, doi: 10.15866/irecap.v13i4.23184.

[13] C. R. Jetti *et al*., "Design and Analysis of Modified U-Shaped Four Element MIMO Antenna for Dual-Band 5G Millimeter Wave Applications," *Micromachines*, vol. 14, no. 8, p. 1545, 2023, doi: 10.3390/mi14081545.

[14] V. Pravalika, S. A. Huq, N. S. Nagu, M. G. Krishna, and G. K. Babu, "Metamaterial-Based Highly Isolated MIMO Antenna for Portable Wireless Applications," *International Journal of Engineering Technology and Management Sciences*, vol. 6, pp. 86–91, 2022, doi: 10.46647/ijetms.2022.v06si01.017.

[15] J. Shah and P. Vasisht, "A Novel Metamaterial Inspired Microstrip Patch Antennas for 5G Applications," in *Proceedings of the International Conference on Smart Systems and Technologies in Electrical and Electronics Paradigms (SSTEPS)*, 2022, pp. 233–236, doi: 10.1109/SSTEPS57475.2022.00065.

[16] M. L. Hakim *et al*.," Metamaterial physical property utilized antenna radiation pattern deflection for angular coverage and iso-

lation enhancement of mm-wave 5G MIMO antenna system," *Radiation Physics and Chemistry*, vol. 209, p. 110998, 2023, doi: 10.1016/j.radphyschem.2023.110998.
[17] X. Cao, Y. Xia, L. Wu, and X. Wu, "Tri-band MIMO antenna design based on characteristic modes manipulation," *AEU - International Journal of Electronics and Communications*, vol. 155, p. 154318, Oct. 2022, doi: 10.1016/j.aeue.2022.154318.
[18] A. Armghan *et al*., "Design and Fabrication of Compact, Multiband, High Gain, High Isolation, Metamaterial-Based MIMO Antennas for Wireless Communication Systems," *Micromachines*, vol. 14, no. 2, p. 357, 2023, doi: 10.3390/mi14020357.
[19] A. K. Singh, S. K. Mahto, and R. S. Sinha, "A Micro Scaled Dual Element MIMO Antenna with Improved Isolation for Terahertz Applications," in *Proceedings of the IEEE India Conference (INDICON)*, Kochi, India, 2022, pp. 1–4, doi: 10.1109/INDICON56171.2022.10040111.
[20] S. Nej, A. Ghosh, S. Ahmad, A. Ghaffar, and M. I. Hussein, "Compact Quad Band MIMO Antenna Design with Enhanced Gain for Wireless Communications," *Sensors*, vol. 22, no. 19, p. 7143, 2022, doi: 10.3390/s22197143.
[21] B. Ramamohan and M. S. G. Prasad, "Design of the MIMO Antenna Using Metamaterial for S-Band Applications, with Reduced Mutual Coupling and Improved Diversity Gain," in *Recent Trends in Communication and Intelligent Systems: Proceedings of ICRTCIS 2021*, Singapore: Springer Nature, 2022, pp. 197–205, doi: 10.1007/978-981-19-1324-2_22.
[22] C. Cui, Y. Ren, P. Tao, and B. Cao, "Microstrip Antenna with High Gain and Strong Directivity Loaded with Cascaded Hexagonal Ring-Shaped Metamaterial," *Materials*, vol. 14, no. 23, p. 7289, 2021, doi: 10.3390/MA14237289.
[23] K. S. Muttair, O. A. Shareef, A. M. A. Sabaawi, and M. F. Mosleh, "Design of multiple-input and multiple-output antenna for modern wireless applications," *TELKOMNIKA Telecommunication Computing Electronics and Control*, vol. 20, no. 1, pp. 34–42, Feb. 2022, doi: 10.12928/telkomnika.v20i1.19355.
[24] A. Wulandari, T. Supriyanto, A. Hasna, R. N. N., and A. Hikmaturokhman, "Performance Analysis of 4×4 MIMO and 8×8 MIMO Antenna Implementation of Private 5G Networks in Industrial Area," *Journal of Informatics and Telecommunication Engineering*, vol. 7, no. 2, pp. 555–565, 2024, doi: 10.31289/jite.v7i2.10440.
[25] J. Vijayalakshmi, V. M. Vinod, V. Dinesh, N. Jeevanantham, J. Haripriya, and K. Jayasurya, "Design and Comparative Analysis of Various Antenna Array Structures for 5G Applications," in *Proceedings of the IEEE International Conference on Computing, Communication and Networking Technologies (ICCCNT)*, Kamand, India, 2024, pp. 1–8, doi: 10.1109/ICCCNT61001.2024.10726103.

BIOGRAPHIES OF AUTHORS

Priethamje Vithya K holds a B.E. in Electronics and Communication Engineering from Madras University in 2004. She received master degree in Digital Communication and Networking from SRM University in 2006. With approximately 14 years of teaching experience, currently she has contributed significantly to academia and research in her field. She can be contacted at email: priethamjevithya@gmail.com.

Varalakshmi L M is Professor at the Department of Electronics and Communication Engineering at Sri Manakula Vinayagar Engineering College, Puducherry, India. She is currently heads the Department of Instrumentation and Control Engineering at Sri Manakula Vinayagar Engineering College, Puducherry, India. She obtained her B.E. (ECE) from Madras University, M.Tech. and Ph.D. in Electronics and Communication Engineering from Pondicherry University. She has about 24 years of teaching experience. Her research are includes wireless communication and image processing. She can be contacted at email: varalakshmi@smvec.ac.in.